Fine tuning of quantum dots photocatalysts for the synthesis of tropane alkaloid skeletons

Ali Dabbous,[a] Eloïse Colson,[b] Debargha Chakravorty,[a] Jean-Marie Mouesca,[a] Christian Lombard,[a] Sylvain Caillat,[a] Jean-Luc Ravanat,[a] Fabien Dubois,[c] Fabrice Dénès,*[b] Philippe Renaud,*[b] and Vincent Maurel*[a]

a) Univ. Grenoble Alpes, CEA, CNRS, IRIG, SyMMES, 38000 Grenoble, France

b) University of Bern, Department of Chemistry, Biochemistry and Pharmaceutical Sciences (DCBP), Freiestrasse 3, CH-3012 Bern, Switzerland

c) Univ. Grenoble Alpes, CNRS, Grenoble INP, Institut Néel, 38000 Grenoble, France

emails for correspondence:

vincent.maurel@cea.fr , philippe.renaud@unibe.ch , fabrice.denes@unibe.ch

Abstract

Several types of Quantum Dots (QDs) (CdS, CdSe and InP, as well as core-shell QDs such as type I InP-ZnS, quasi type-II CdSe-CdS and inverse type-I CdS-CdSe) were considered for generating α-aminoalkyl free radicals. The feasibility of the oxidation of the *N*-aryl amines and the generation of the desired radical was evidenced experimentally by quenching of the photoluminescence of the QDs and by testing a vinylation reaction using an alkenylsulfone radical trap. The QDs were tested in a radical [3+3]-annulation reaction giving access to tropane skeletons and that requires the completion of two consecutive catalytic cycles. Several QDs such as CdS core, CdSe core and inverted type I CdS-CdSe core-shell proved to be efficient photocatalysts for this reaction. Interestingly, the addition of a second shorter chain ligand to the QDs appeared to be essential to complete the second catalytic cycle and to obtain the desired bicyclic tropane derivatives. Finally, the scope of the [3+3]-annulation reaction was explored for the best performing QDs and isolated yields that compares well with classical iridium photocatalysis were obtained.

Introduction

Visible light photoredox catalysis with transition metal complexes (mainly based on Ir and Ru complexes) and organic photocatalysts has developed rapidly during the last two decades, resulting in impressive development in the field of organic synthesis.[1–7] Besides, semiconductor quantum dots (QDs) start to appear as efficient photocatalysts for CO_2 reduction[8–10] and H_2 production,[11–13] as well as at promoting synthetic organic transformations, as demonstrated by some of us[14] and several others groups,[15–21] relying in the majority of cases on CdS and CdSe QDs.

The different main types of core and core-shell QDs structures used in photoredox catalysis are presented in Figure 1. The efficiency of the charge transfer between the QDs and a substrate (electron donor or acceptor) primarily depends on the accessibility to the charge carriers delocalized in the QDs. In the case of core QDs (Figure 1A), both hole (h) and electron (e) can reach the surface and are well accessible to substrates. The main limitation for the charge transfer is the short lifetime of photoexcited QDs due to charges recombination (typically 10-20ns in core QDs). In the case of core-shell structured QDs (Figure 1B–1E) the distribution of the charges depends on the alignment of the energy bands edge of the core and the shell. According to this alignment in the core-shell QDs, the core-shell structures of interest in this study are classified into four main types: type-I (Figure 1B), inverted type-I (Figure 1, C), type-II (Figure 1D) and quasi type-II (Figure 1E).[22,23] In type-I QDs, such as InP-ZnS, the band gap of the core is smaller than that of the shell, and the position of the energy bands of the band gap of the core falls within that of the shell (Figure 1B). This makes the generated charge carriers localized in the core of the type-I QDs and consequently can induce difficult accessibility during the charge transfer process. On the opposite, in the inverted type-I QDs, such as CdSe-CdS[24–26] the band gap of the core is larger than that of the shell, and the energy bands edges of the shell are aligned within that of the core (Figure 1C)). In such a case, the generated charges are expected to be delocalized in the outer shell of the QDs, which can enhance their interaction with the substrates. In the case of type-II core-shell QDs (or quasi type-II[24]), the valence band edge of the core is aligned within the band gap of the shell, and the conduction band edge of the shell falls within the band gap of the core (type II, Figure 1D) or very close to the conduction band of the core (quasi-type II, such as CdSe-CdS) (Figure 1E). The hole is maintained in the core of the QDs and is less accessible to substrates, while the electron is localized in the outer shell (type II) or delocalized between the core and the shell (quasi type II) and is more accessible to substrates. This can result in a better charges separation, with longer lifetimes (up to 200 ns[27]).

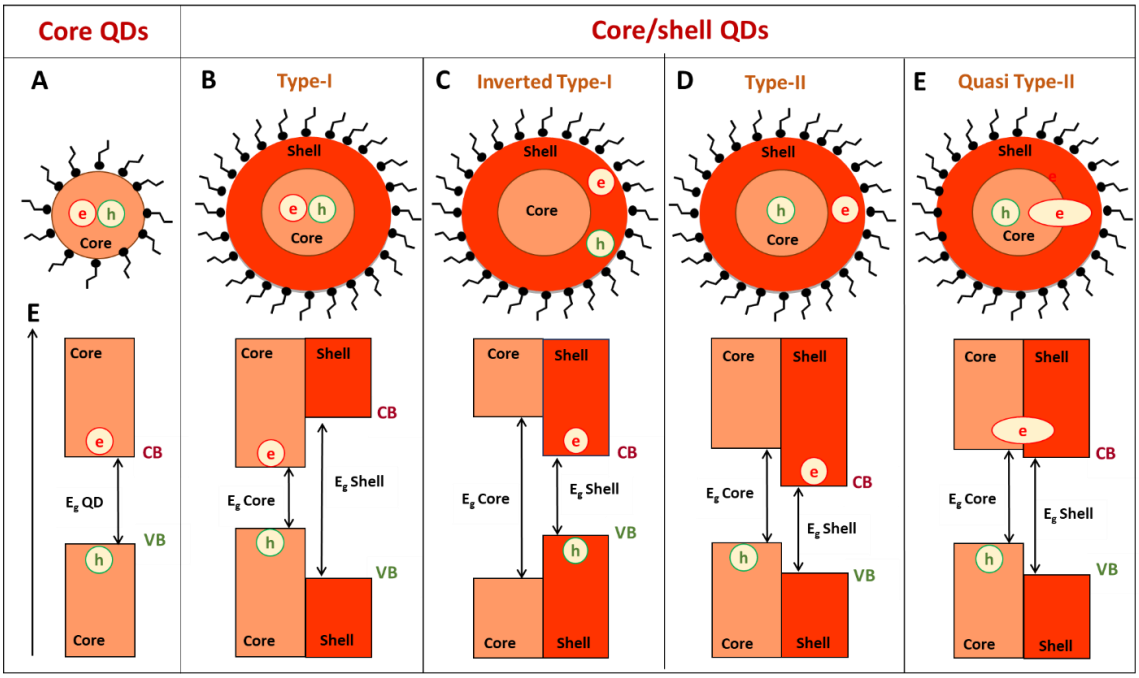

Figure 1. Energy levels and charges localization in different types of QDs. Upper part: distribution of the charges after the photoexcitation of the different types of QDs. Lower part: conduction and valence bands alignment in the different types of QD. h stands for hole, e for electron, E_{CB} for the energy of the conduction Band, E_{VB} for the energy of the Valence Band and E_g for the band gap energy.

Simple CdS and CdSe QDs have been used for multiple C–C bond formation as exemplified by the decarboxylative radical addition to styrene reported by Krauss,[28] and the cascade cyclisation reaction of difluorochlorides reported by Feng.[29] A few other QDs structures were investigated in order to improve the reactivity of the photogenerated electrons in C–C bond formation reactions following reductive pathways. QDs made of semiconductors with more reductive conduction band edge levels, such as ZnSe and $CuInS_2$, were reported for the C–C bond formation by reduction of aryl halides[30] and for the removal of protecting groups.[31] The use of CdSe-CdS quasi type-II QDs (Figure 1E) enabled Peng and co-workers to achieve the reduction of imines[32] and the pinacol coupling of aldehydes and ketones[33] with outstanding turnover numbers (TON > 4×10^5).

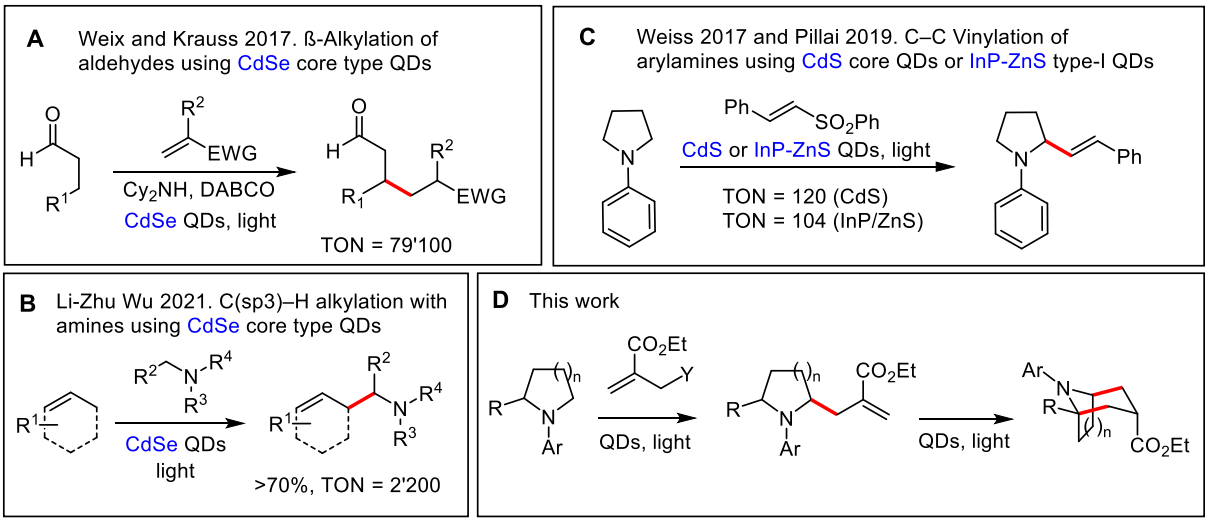

Scheme 1. Photoredox catalyzed reactions using quantum dots.

Since the seminal work of Weix and Krauss on the QDs-photocatalyzed alkylation of aldehydes (Scheme 1A),[28] the vast majority of QDs-photocatalyzed C–C bond formation reactions following oxidative pathways still rely on core CdSe or CdS QDs for providing the photogenerated holes with an appropriate reactivity for the targeted reaction. For instance, Li-Zhu Wu and co-workers reported recently examples of C–C bond formation reactions[34–36] based on a dual one-electron oxidation of tertiary amines and alkenes (Scheme 1B). In another seminal work, Weiss and co-workers reported the α-vinylation of *N*-arylamines (Scheme 1C) with core CdS[37] and later Pillaï and co-worker reported the same reaction with type-I core-shell InP-ZnS QDs (see Scheme 1 and Figure 1).[38] Besides this unique example of reaction reported with two different types of QDs, up to now, no investigation was reported about the photocatalysis of such an oxidative pathway reaction using different core-shell QDs structures (see Figure 1) that would induce either a better charge separation (such as type-II or Quasi type-II QDs) or localize both charge in the outer shell in order to make them more reactive (such as inverted type-I QDs).

Recently, our groups reported a unique photoredox catalyzed synthesis of tropane and related alkaloid skeletons via a radical [3+3]-annulation process (Scheme 1D).[39] The reaction involves two successive photocatalyzed one-electron oxidation of an arylamine to generate α-aminoalkyl radicals (Scheme 1D). The limited number of QDs structures investigated up to now for reactions following an oxidative pathway prompted us to perform a systematic study of several types of QDs to perform the radical [3+3]-annulation. We report here that several different types of QDs are suitable for this transformation and that enhanced reactivity can be achieved by QD ligand exchange.

Result and discussion

A. Charge transfer between QDs and 1-phenylpyrrolidine (**1a**)

At first, three types of core QDs, CdS, CdSe and InP were considered for generating the α-aminoalkyl free radical by comparing the reported potentials of the valence band edge of the QDs to the DFT computed one-electron oxidation potential of the *N*-arylamine model substrate 1-phenylpyrrolidine (**1a**) (Table 1). The one-electron oxidation potential of **1a** was computed to be E°= +0.57 V vs. SCE (+0.81 V vs. NHE) in acetonitrile as a solvent and E°= +0.64 V vs. SCE (0.88 V vs. NHE) in trifluorotoluene (TFT), which was selected in this study as a less volatile alternative to dichloromethane. The reported values for the valence band of CdS QDs vary between +1.24 V vs SCE[40] to +1.66 V vs SCE[37] for CdS QDs and between +0.66 and +1.20 V vs SCE for CdSe QDs depending on their size and their surface ligands.[41] The valence band edge of InP QDs was estimated to be +1.09V vs. SCE[38,42] and +1.75 V vs.SCE[38,42]. Overall, as presented in Table 1, the valence band of CdS, and InP QDs are higher than +1.00 V vs. SCE, so they have a good driving force (typically > 0.4 V) for the oxidation process. For CdSe QD the position of the valence band can be as low as 0.66 V vs. SCE so the driving force can range from 0.56 V down to 0.02 V and might be too low for the one-electron oxidation.

Table 1. Comparison between Valence Band (VB) edge redox potentials and the redox potential of **1a** computed by DFT (TFT as a solvent).

QDs	VB (V vs. SCE)	E°($1a^{+\bullet}$/1a V vs. SCE)	Driving Force (V)
CdS	1.24[40]–1.66[37]	0.64	> 0.60
CdSe	0.66[41]–1.20[41]	0.64	> 0.02
InP	1.09[42]–1.75[38]	0.64	> 0.45

Then the QDs considered for this study, including core CdS[43], CdSe[44], InP[45] (simply called CdS, CdSe, InP in the text) different types of core-shell QDs type I InP-ZnS[45] (called InP-ZnS), quasi type-II CdSe-CdS[46] (called CdSe-CdS) and inverted type-I CdS-CdSe[25,26] (called CdS-CdSe) were synthesized according to literature procedures with slight modifications for each type of QDs (see SI S1), and characterized by UV-visible spectroscopy (see SI Figures S1.1) , fluorescence (see SI Figures S1.2) spectroscopy and TEM microscopy (see SI Figures S1.3, S1.4 and S1.5).

The possibility of the charge transfer from the QDs to **1a** was studied by performing photoluminescence quenching experiments. All the tested QDs showed a quenching of photoluminescence after adding 5 mM of **1a** as evidenced by the corresponding Stern-Vollmer plots

(see Figure 2). InP core QDs were not tested as they are not photoluminescent. Three types of QDs, namely CdS, CdSe and CdS-CdSe exhibited a strong photoluminescence quenching with Stern-Vollmer constants in the range 183–314 mol L^{-1} (see SI section S.2) while CdSe-CdS and InP-ZnS exhibited less strong quenching, but with non-negligible Stern-Vollmer constants in the range 51–98 mol L^{-1}. So, from the photoluminescence quenching measurements, it appears that all the considered QDs can perform an efficient charge transfer to **1a** and that CdS, CdSe and CdS-CdSe QDs interact more efficiently with **1a** than CdSe-CdS and InP-ZnS QDs, most probably because in the two latter core-shell structures (quasi type II and type I, respectively) the photogenerated hole is located in the core and so is less accessible to the substrate (see Figure 1E and 1B, resp.).

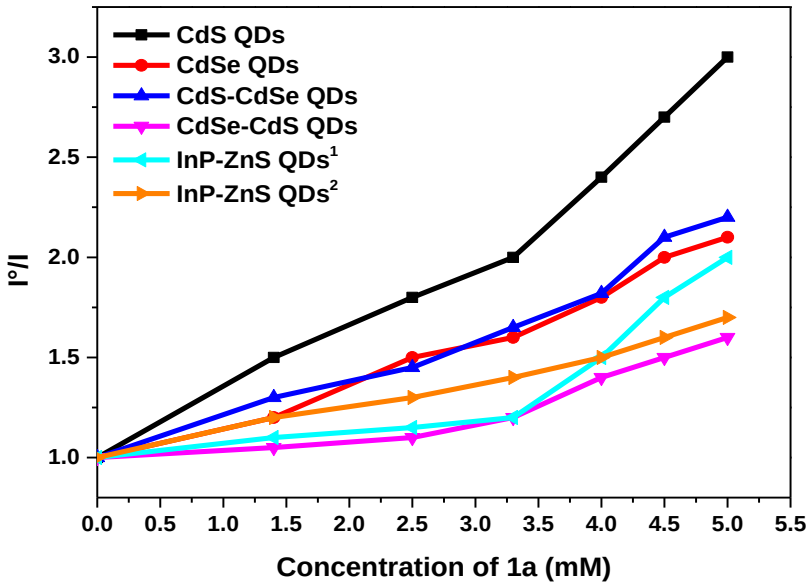

Figure 2. Photoluminescence quenching of the QDs by **1a.** Stern-Vollmer plots computed from the photoluminescence plot (see SI 2 for details) of the QDs in presence of **1a** (up to 5 mM) in TFT. [1)]Oleylamine capped InP-ZnS QDs. [2)]Commercial oleate capped InP-ZnS QDs.

B. Low scale photocatalysis (1 µmol of 1a)

Vinylation and [3+3] annulation involving 1a

The QDs were first tested with the one-step α-vinylation reaction previously reported by MacMillan with an Ir(III)-based complex,[47] then later by the Weiss and Pillai groups using CdS QDs[37] and InP-ZnS QDs,[38] respectively. This well-established reaction proceeds via a radical mechanism closely related to that of the first cycle of the [3+3] annulation reaction. The oxidation of **1a** to the corresponding aminyl radical cation, followed by deprotonation, ultimately generates an α-aminoalkyl radical that reacts

with the 2-phenylethenylsulfone radical trap. All different QDs were tested in trifluorotoluene (TFT) with **1a** (1 µmol) and the radical trap (1.1 µmol). The concentration of the QDs in each reaction was set based on their calculated extinction coefficient (see SI table S.3) and targeting an absorbance close to 1.

CdS, CdSe and CdS-CdSe were tested first. CdS QDs functionalized with their native oleate surface ligands possess a high extinction coefficient close to 10^6 m^{-1} cm^{-1} (see SI table S.3), which offers the possibility of using a low catalytic loading (0.1 mol%). They afforded the vinylated pyrrolidine **2** in 49% after 4 h of irradiation at 455 nm (Table 2, Entry 1), which is similar to the yield reported by Zhang et al[37] (50% using 0.5 mol% CdS QDs after 7.5 h of irradiation). CdSe QDs (0.5 mol%) gave **2** in 51% yield upon irradiation at 528 nm for 4 hours (Table 2, entry 2). Similarly, CdS-CdSe QDs (0.5 mol %) functionalized with oleylamine as surface native ligands provide **2** in 48% yield upon irradiation at 528 nm for 4 hours (Table 2, entry 3). The other types of QDs investigated, namely CdSe-CdS, InP and InP-ZnS exhibited a slower kinetics (see SI Figure S5.1A and S5.1B) and provided **2** in 30%–43% yields after 6 h of irradiation (Table 2, entries 4–6). Noteworthy, the use of the commercially available oleate capped InP-ZnS QDs resulted in 43% yield in 6 hours of irradiation (Table 2, Entry 7), which is close to the results reported by Pillai[38] (52 % after 10 hours of irradiation). For all the studied QDs, our attempts to increase the irradiation time (up to 22 hours) only led to a degradation of the vinylation product **2**, which was attributed to an over-oxidation leading to by-products, as proposed by Zhang et al.[37]

Table 2. Screening the activity of the QDs. All the reactions are run on the 0.001 mmol scale in TFT. The reaction products **2**, **3a** and **4a** are quantified by UHPLC-MS by comparison with authentic samples.

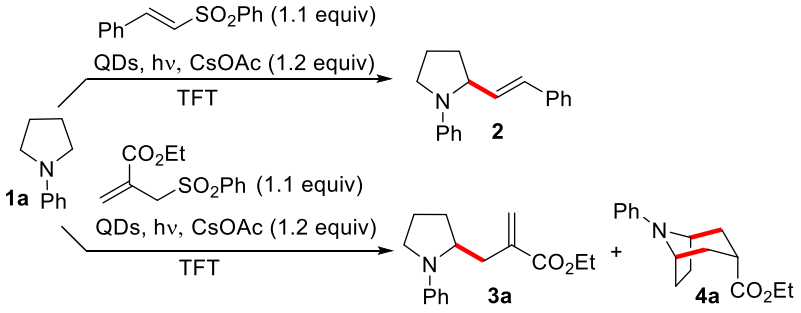

Entry	QDs *type*	Surface ligands	Catalyst loading	λ_{irr}[1]	Vinylation Yield 2 (time)	[3+3] Annulation Yield 3a/4a (time)
1	CdS *core*	oleate	0.1%	455 nm	49% (4 h)	52%/12% (24 h)
2	CdSe *core*	oleate	0.5%	528 nm	48% (4 h)	49%/6% (24 h)
3	CdS-CdSe inverted type I	oleylamine	0.5%	528 nm	51% (4 h)	59%/15% (24 h)
4	CdSe-CdS quasi type II	oleylamine	0.5%	528 nm	30% (6 h)	42%/11% (24 h)
5	InP *core*	oleylamine	0.7%	455 nm	40% (6 h)	30%/n.d[3] (24 h)
6	InP-ZnS *type I*	oleylamine	0.7%	455 nm	42% (6 h)	42%/n.d.[3] (48 h)
7	InP-ZnS *type I*	oleate[2]	0.7%	528 nm	43% (6 h)	38%/n.d.[3] (24 h)

[1]irradiation power: 528 nm: 50 mW; 455 nm: 10 mW. [2] Commercially available; [3] n.d. = not detected

The ability of the QDs to photocatalyze a [3+3] annulation reaction involving two consecutive redox neutral cycles was investigated next. For this purpose, **1a** (1 μmol) was allowed to react with ethyl 2-((phenylsulfonyl)methyl)acrylate (1.1 equivalents) under the reaction conditions developed for the alkenylation reaction. For all studied QDs, 24 h of irradiation provided the intermediate allylated pyrrolidine **3a** in 42%–59% yields (Table 2). Interestingly, formation of the desired bicyclic product **4a** was observed with CdS, CdSe, CdS-CdSe and CdSe-CdS QDs (Table 2, entries 1–4), albeit in low yields (≤15%). Reactions with InP or InP-ZnS QDs stopped at the allylated product **3a** without formation of bicyclic **4a** even after 48 hours of irradiation. Based on these initial results, we decided to optimize the QDs by modifying the ligand layer.

Enhancing QDs photocatalytic activity by partial or complete ligand exchange with shorter ligands

The QDs were prepared with long-chain ligands such as oleate or oleylamine on their surface, which can hinder the access of the reaction substrate to the QDs[48]. It was reported by Zhang et al.[37] that a partial exchange of oleate ligands on CdS QDs with shorter *n*-octyl phosphonate ligands enabled to increase the initial rate of the vinylation reaction by a factor of 2.3. This was attributed to disorder in the ligand layer created by the presence of two different ligands, that helps the substrate to reach the surface of the QDs (Figure 3A). Moreover, Wang at al.[49] and Weidman et al.[50] reported that QDs surrounded by shorter ligands, or by a blend of ligands of two different sizes, are better dispersed.

The effect of the partial exchange of oleate with shorter octyl phosphonate ligands was first investigated for CdS and CdSe core QDs on the reaction leading to the tropane framework **4a**. The partial exchange was obtained by adding *n*-octyl phosphonic acid (*n*-$C_8H_{17}PO_3H_2$) to the QDs one hour before performing the photocatalytic reaction, without further treatment. Under these conditions, a strong increase of photocatalytic performance was observed for CdS and CdSe QDs. The yield of **4a** increased from 12% to 75% by treating the CdS QDs with 380 equivalents of *n*-$C_8H_{17}PO_3H_2$ and from 6% to 73% by treating CdSe QDs with 300 equivalents of *n*-$C_8H_{17}PO_3H_2$ (Figure 3B). For CdS QDs, the reaction kinetics is presented in Figure 3C. Complete consumption of the starting material **1a** occurs within 10 hours of irradiation. Formation of the mono-allylated intermediate **3a** was reached after 9 hours while formation of **4a** needed 24 hours of irradiation to reach its maximum.

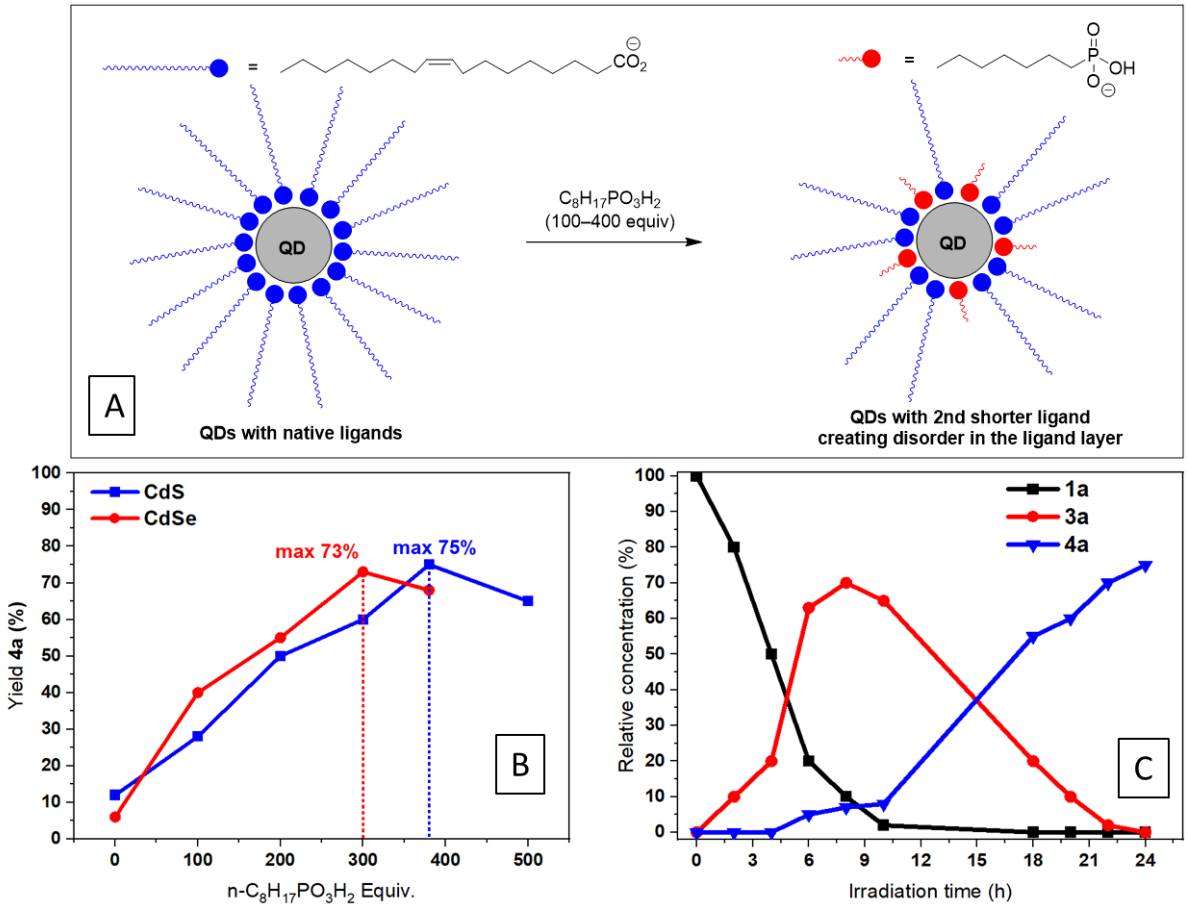

Figure 3. Effect of the addition of *n*-octylphosphonic acid on CdS and CdSe QDs. A) Ligand exchange process. B) Effect on the yield of **4a**. C) Reaction kinetics using CdS QDs with the optimal quantity (380 equiv.) of *n*-octylphosphonic acid.

Then, the CdS QDs were tested for successive uses with only one initial treatment with *n*-$C_8H_{17}PO_3H_2$. The first and second runs provided **4a** in 73% yield and 75% yield respectively. However, the third run showed a decreased yield of 63% (see also SI section S.6).

Encouraged by the spectacular enhancement obtained with CdS and CdSe QDs for the formation of **4a**, the partial ligand exchange was tested for other types of QDs for the vinylation leading to **2** and the annulation leading to **4a**. The results are summarized in Table 3 (Table 3, entries 1–7). For core CdS and CdSe QDs, the partial exchange of oleate with *n*-octylphosphonate ligands lead also to a significant improvement for the vinylation reaction. The use of 0.1 mol% CdS QDs treated with *n*-$C_8H_{17}PO_3H_2$ (380 eq) led to **2** in 68% yield after 3 h of irradiation (Table 3, entry 1) compared to 49% after 4 h for the non-modified QDs (Table 2, entry 1). This result compares well with the yield obtained by Zhang et al. after modifying the QDs surface with a similar addition of *n*-octylphosphonate ligands (60% yield using 0.5 mol% catalytic loading). The quantum yield (QY) was measured by ferrioxalate actinometry (see SI section S.7.3) to be 0.18%, a value comparable to that reported by Zhang et al. (0.22%).[37] Similarly, CdSe QDs treated with 300 equiv of *n*-$C_8H_{17}PO_3H_2$ afforded the vinylated product **2** in 70 % yield (Table

3, entry 2) compared to 51% for the non-modified QDs (Table 2, entry 2). Beside CdS and CdSe QDs, CdS-CdSe QDs also exhibited a strong enhancement of their photocatalytic activity for both reactions (Table 3, entry 3). The use of CdS-CdSe QDs (0.5 mol%) treated with 400 eq of *n*-$C_8H_{17}PO_3H_2$ resulted in high yields for both reactions (74% for **4a** and 69% for **2**) (Table 3 entry 3) comparing with 15% (**4a**) and 51% (**2**) yields obtained with the non-modified QDs (Table 2, entry 3). These last results show that the partial ligand exchange with *n*-$C_8H_{17}PO_3H_2$ is not limited to oleate coated QDs (CdS, CdSe) but is also efficient when the initial ligand is oleylamine (CdS-CdSe).

The use of 0.5 mol% of CdSe-CdS treated with 400 equivalents of *n*-$C_8H_{17}PO_3H_2$ lead to a very slight yield improvement for **2** (33%, Table 3, entry 4) compared to the reference reaction (30%, Table 2, entry 4). The annulation reaction gave a mixture of **3a** (42%) and **4a** (13%) (Table 3, entry 4) similar to the one observed without ligand exchange (Table 2, entry 4). The use of 0.7 mol% of InP QDs treated with 500 eq of *n*-octylamine (Table 3, entry 5) provided no change relative to the native InP QDs (Table 2, entry 5) for both reactions. For InP-ZnS QDs, the addition of a shorter ligand was tested by adding octylamine to oleylamine capped QDs (Table 3, entry 6) and by adding *n*-$C_8H_{17}PO_3H_2$ to oleate capped QDs (Table 3, entry 7). For both catalysts, the vinylation reaction leading to **2** proceeded with similar yields, 44% and 46% respectively, as the one with unmodified catalysts (Table 2, entries 6 and 7). Attempts to run the annulation process provided exclusively the allylated pyrrolidine **3a** with slightly higher yields (48% and 45%, resp. vs. 42% and 38% without ligand exchange). These results suggest that InP-ZnS QDs are promising catalysts to perform the simple allylation reaction. This selectivity may tentatively be attributed to the limited reducing power of their conduction band[38,42] that does not allow the final reduction of the bicyclic α-ester radical (see discussion of the mechanism, vide infra).

At last, complete ligand exchange was tested for CdS and CdSe QDs using 500 equivalents of phosphonopropanoic acid ($HO_2C(CH_2)_2PO_3H_2$). The use of $HO_2C(CH_2)_2PO_3H_2$ was reported to transfer QDs into water using dimethylformamide as an intermediate polar solvent.[51] After treatment with $HO_2C(CH_2)_2PO_3H_2$, CdS and CdSe core QDs could be dispersed in acetonitrile (ACN) and then their photocatalytic activity was tested (Table 3, entries 8 and 9). The vinylation reaction gave **2** in 67% and 71% using CdS and CdSe, respectively. The annulation reaction gave, after 24 h of irradiation, **4a** in a 74% and 72% yield using CdS and CdSe QDs, respectively. However, it was observed that after 24 hours of reaction under light irradiation in acetonitrile, the phosphonopropanoate coated QDs lost their optical properties (see SI section S6). Their poor stability makes them unsuitable for recycling and they have not been further investigated.

Table 3. Screening the photocatalytic activity of QDs after exchange with shorter ligands. All the reactions are run on the 1 µmol scale in TFT. The reaction products **2**, **3a** and **4a** are quantified by UHPLC-MS by with authentic samples. Conditions of irradiation: 50 mW at 528 nm for CdSe, CdS-CdSe, CdSe-CdS and InP-ZnS (Oleate), 10 mW at 455 nm for CdS, InP and InP-ZnS (Oleylamine).

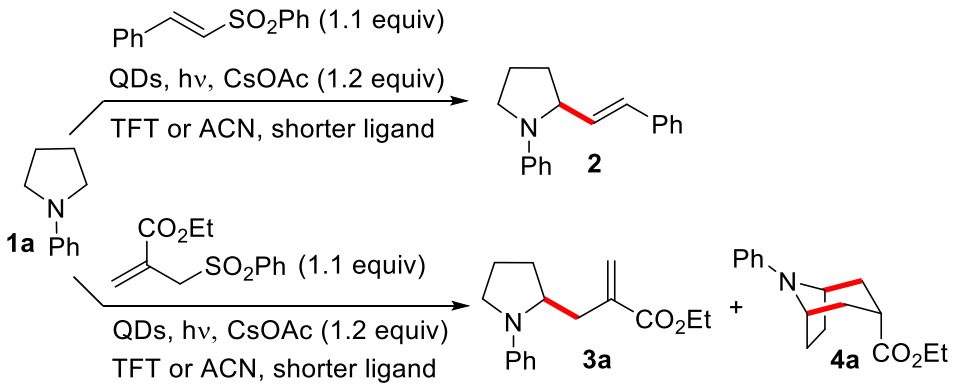

Entry	QDs *type*	Native ligand	Added shorter ligands (equiv)	Solvent	Catalyst loading	Vinylation Yield 2	[3+3] Annulation Yield 3a/4a[1]
1	CdS	oleate	*n*-$C_8H_{17}PO_3H_2$ (380)	TFT	0.1%	68% (3 h)	n.d./75% (24 h)
2	CdSe	oleate	*n*-$C_8H_{17}PO_3H_2$ (300)	TFT	0.5%	70% (4 h)	n.d./73% (24 h)
3	CdS-CdSe	oleylamine	*n*-$C_8H_{17}PO_3H_2$ (400)	TFT	0.5%	69% (4 h)	n.d./74% (24 h)
4	CdSe-CdS	oleylamine	*n*-$C_8H_{17}PO_3H_2$ (400)	TFT	0.5%	33% (6 h)	42%/13% (24 h)
5	InP	oleylamine	*n*-octylamine (500)	TFT	0.7%	42% (6 h)	32%/n.d. (24 h)
6	InP-ZnS	oleylamine	*n*-octylamine (500)	TFT	0.7%	44% (6 h)	48%/n.d. (48 h)
7	InP-ZnS	oleate	*n*-$C_8H_{17}PO_3H_2$ (500)	TFT	0.7%	46% (6 h)	45%/n.d. (24h)
8	CdS	oleate	$HO_2C(CH_2)_2PO_3H_2$ [(2)]	ACN	0.1%	67% (3h)	n.d./74% (24h)
9	CdSe	oleate	$HO_2C(CH_2)_2PO_3H_2$ [(2)]	ACN	0.5%	71% (3h)	n.d./74% (24h)

[1)] n.d. = not detected, [2)] 500 equivalents of shorter were added with a phase transfer to DMF then to ACN (see main text)

In summary, partial exchange of the native oleate and oleylamine ligands at the surface of the CdS, CdSe and CdS-CdSe QDs with the smaller *n*-octylphosphonate ligand proved to efficiently promote their efficiency for the two reactions under investigation. This effect is particularly impressive in the case of the [3+3] annulation leading to **4a**. With all other QDs examined, this ligand exchange process had either no effect or only a limited positive effect on the catalyst efficiencies.

C. Scaling-up the [3+3] annulation

Optimization of the preparation of **4a** with CdS, CdSe and CdS-CdSe QDs

After having successfully developed the QDs photocatalyzed protocol on the 1 µmol scale, the scalability of the methodology was investigated with CdS, CdSe, and CdS-CdSe QDs. For this study, the synthesized QDs were modified by ligand exchange with *n*-octylphosphonic acid according to Table 3 (entries 1–3). The reactions were performed on 0.05 mmol scale in 4 mL of TFT (12.5 mM). The QDs catalyst loading was decreased to set the absorbance in TFT at A = 3.7 to enable a sufficient penetration of light in the reaction vessel. Promising results were obtained with CdS and CdSe QDs with isolated yields of respectively 42% and 56% for the cyclized product **4a** (Table 4, entries 1 and 2). Although significantly lower than the yields obtained on 1 µmol scale, these yields were obtained with a lower catalyst loading (0.025 mol% vs. 0.1 mol% for CdS, 0.16 mol% vs. 0.5 mol% for CdSe). A high TON of 1680 was obtained for CdS QDs while CdSe QDs showed a lower efficiency (TON of 350). The reaction run with CdS-CdSe QDs was significantly less clean and **4a** was isolated in a low 21% yield after 24 h of irradiation corresponding to TON of 131 (Table 4, entry 3). No significant amounts of starting material or side-product was observed that could explain the low yield of the annulation reaction. Considering these results, CdS QDs which exhibited high yield and good TON at low catalyst loading were selected as the most promising candidate for further optimization of the scale-up process.

Table 4. Optimization of the reaction conditions on 0.05 mmol (12.5 mmol) scale using the sulfone trap.

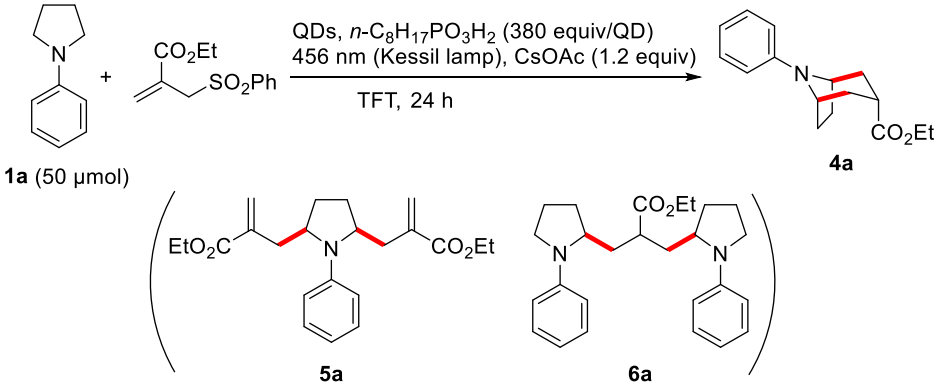

Entry	QDs type	Catalyst Loading	Abs	Radical trap	Isolated yield of 4a[1]	TON	Side product
1	CdS	0.025%	3.7	1.1	42%, α/β 4.5:1	1680	**6a**
2	CdSe	0.16%	3.7	1.1	56%, α/β 6:1	350	none
3	CdS-CdSe	0.16%	3.7	1.1	21%, α/β 4.5:1	131	Unidentified
4	CdS	0.025%	3.7	1.4	27% (α only)	1080	**6a**, **5a**
5	CdS	0.05%	7.4	1.1	~50%[2]	1000	**6a**
6	CdS	0.05%	7.4	1.4	49% (α/β 5:1)	980	none
7	CdS	0.05%	7.4	1.4	36% (α)	720	**6a**
8	CdS	0.05%	7.4	2.0	traces		**5a**

[1)] Irradiation with one Kessil lamp (100 W) for 24 hours (at 456 nm CdS QDs and at 525 nm for CdSe and CdS-CdSe QDs). Experiments performed in TFT with appropriate amounts of OPAc ligands determined in section B-2. Reactions were set-up inside the glovebox and irradiated with one Kessil lamp outside the glovebox. When applicable, ^{1}H-NMR yield was determined using ethylene carbonate as a standard. [2)] Approximate NMR yield due to unclean reaction; difficulties of purification prevented isolation of the product.

Although encouraging result was obtained with 0.025 mol% CdS and 1.1 equivalents of the sulfone trap (Table 4, entry 1), the presence of side product **6a** not only decreased the yield of the desired cyclized product but also greatly impaired its purification due to the very similar polarity. Since this side product is formed when too little trap is present, the reaction was repeated with 1.4 equivalents of the allylsulfone radical trap (Table 4, entry 4). Under these conditions, formation of both **5a** and **6a** was observed and the major diastereomer of **4a** was isolated in only 27% yield. Next, QDs catalyst loading was doubled while keeping the concentration of substrate unchanged at 12.5 mM. The increase of the absorbance up to 7.4 was well-tolerated and a significant amount of **4a** (~50%) was detected by ^{1}H-NMR analysis of the crude mixture (Table 4, entry 5). However, the presence of **6a** did not permit to isolate pure **4a**. Increasing the quantity of radical trap to 1.4 equivalents proved beneficial and **4a** was isolated in 49% yield (Table 4, entry 6). Unfortunately, the reaction was poorly

reproducible and in a duplicate experiment, the major diastereomer was isolated in 36% yield along with **6a** (Table 4, entry 7). In the iridium-catalyzed reaction, it was observed that the sulfone radical trap was not stable over long reaction time.[39] While this does not affect the iridium-catalyzed reaction due to short reaction times, it might explain why **6a** was formed in most of our reactions. Running the reaction with 2.0 equivalents of the allylic sulfone was performed but led mainly to the formation of the bisallylated product **5a** (Table 4, entry 8).

Exploring the scope of radical trap

The iridium photocatalyzed [3+3] annulation process was performed with a series of allylic radical traps such as allyl sulfones (Y = SO_2Ph), allyl acetate (Y = OAc) and allyl thioether (Y = S-*tert*-dodecyl) and best results were obtained with the acetate.[39] Therefore, the influence of the leaving group Y on the radical traps was examined for the CdS and CdSe QDs photocatalyzed [3+3] annulation at 1 µmol scale. The use of an allyl acetate (Y = OAc) instead of an allyl sulfone (Y = SO_2Ph) radical trap gave similar results in terms of yields and reaction time (Table 5, entries 1 and 2, 72% and 70% yield vs. Table 3, entries 1 and 2, 75% and 73% yield). The thioether radical trap (Y = S-*t*-dodecyl) gave desired cyclized product **4a** in 55% and 50% yield (Table 5, entries 3 and 4).

Table 5. Radical trap screening at low and higher scale for CdS and CdSe QDs

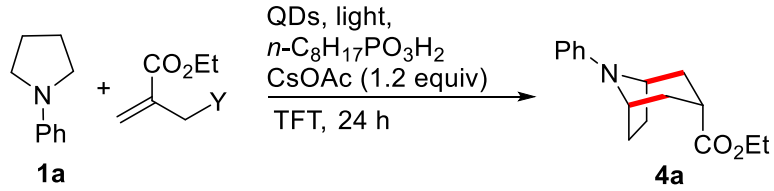

1a **4a**

Entry	QDs	1a (mmol)	cat.load	Abs	Y (equiv)	Yield 4a
1[1]	CdS	0.001	0.1%	1.1	OAc (1.1)	72%
2[1]	CdSe	0.001	0.5%	0.9	OAc (1.1)	70%
3[1]	CdS	0.001	0.1%	1.1	S-*t*-Do (1.4)	55%
4[1]	CdSe	0.001	0.5%	0.9	S-*t*-Do (1.4)	50%
5[2]	CdS	0.05	0.05%	7.4	OAc (1.1)	34% α/β 5:1
6[2]	CdS batch 1	0.05	0.05%	7.4	OAc (1.3)	50% α/β 5:1
7[2]	CdS batch 2	0.05	0.05%	7.4	OAc (1.3)	51%, α/β 5:1
8[2]	CdS batch 3	0.05	0.05%	7.4	OAc (1.3)	58%, α/β 5:1
9[3]	CdS batch 3 - Schlenk	0.05	0.05%	7.4	OAc (1.3)	61%, α/β 5.5:1
10[2]	CdS	0.05	0.025%	3.7	OAc (1.3)	42% α/β 3:1
11[4]	CdS 1st use	0.20	0.05%	7.4	OAc (1.3)	46% α/β 6:1
12[4]	CdS 2nd use	0.20	0.05%	7.4	OAc (1.3)	42% α/β 4:1
13[4]	CdS 3rd use	0.20	0.05%	7.4	OAc (1.3)	35% α/β 4:1

[1)] Reactions were run in a glovebox on the 0.001 mmol scale in 1mL trifluorotoluene and the reaction yield was determined by integrating the UHPLC-MS peaks compared to the peak of the corresponding standard of the reaction products. Time of reaction: 24 hours. Conditions of irradiation: 50 mW LED at 528 nm for CdSe, 10 mW LED at 455 nm for CdS. [2)] Reactions were run at 0.05 mmol scale outside the glovebox, irradiation with one Kessil lamp (100 W) for 24 hours in a 8-mL clear glass vial with a screw cap. [3)] Same reaction conditions as 2 using a tight Schlenk reaction vessel. [4)] Reaction was run at 0.2 mmol scale outside the glovebox, irradiation with two Kessil lamps (100 W) for 24 h in a 20-mL clear glass vial with a screw cap.

The allylic acetate radical trap was further investigated at larger scale (50 µmol) with CdS QDs. The reaction was clean and **4a** was isolated in 34% (Table 5, entry 5). In line with previous observations, increasing the trap equivalent number from 1.1 to 1.3 proved beneficial and the isolated yield was raised to 50% (Table 5, entry 6). With the optimized conditions in hand, the reproducibility of the reaction with different batches of QDs was tested and proved to be excellent with 51 and 58% yields (Table 5, entries 7 and 8). Then, the same reaction with the third batch of QDs was run using a tight reaction vessel (Schlenk type) instead of a simple screw type vials but the yield was only marginally better (Table 5, entry 9, 61%). Reducing the catalyst loading to 0.025 mol% induced a significant decrease in yield (Table 5, entry 10). Finally, the reaction was run on 200 µmol scale under our best reaction conditions to afford **4a** in 46% yield (Table 5, entry 11) reaching a TON of 920. This result is very close to the one reported for the iridium-catalyzed reaction which gave **4a** in 57% yield but with

a TON of only 57.[39] Remarkably, it was possible to recycle the CdS QDs and to perform again the reaction a second and a third times at the same scale with only moderate erosion of the yield (Table 5, entries 12 and 13, 42% and 35% respectively).

[3+3]-Annulation with different *N*-arylamines.

The possibility of expanding the scope of the reaction to other precursors was examined with a short selection of *para*-substituted *N*-arylpyrrolidines and *N*-arylpiperidines, which were found to be suitable partners in the Ir(III) catalyzed reaction.[39] Redox potentials of these precursors were computed by DFT and data are presented in Figure 4. As expected, compared to the non-substituted *N*-phenylpyrrolidine **1a** (+0.64 V vs. SCE in TFT), precursors bearing electron donating groups such as *para*-methoxy-phenylpyrrolidine **1b**, *para*-methyl-phenylpyrrolidine **1c** and the 2-methyl substituted N-phenylpyrrolidine **1d** exhibited lower redox potentials (+0.29, +0.50 and +0.48 V vs. SCE). On the opposite, *p*-carbomethoxy phenylpyrrolidine **1f** bearing an electron withdrawing group exhibited a higher redox potential (+0.89 V vs. SCE). A similar trend was observed with *N*-arylpiperidines: *para*-methoxy-phenylpiperidine **1h** has a lower redox potential (+0.29 V vs. SCE) than the non-substituted phenylpiperidine **1g** (+0.66 V vs. SCE), which has a lower potential than *p*-carbomethoxyphenylpiperidine **1i** and *p*-boropinacolpiperidine **1j**, which bear electron withdrawing groups (+1.00 V vs. SCE and 0.72 V vs. SCE).

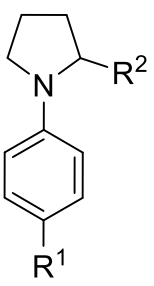

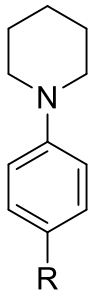

1a R^1 = H, R^2 = H +0.64
1b R^1 = OMe, R^2 = H +0.29
1c R^1 = CH_3, R^2 = H +0.50
1d R^1 =H , R^2 = CH_3 +0.48
1e R^1 =Br , R^2 = H +0.62
1f R^1 =CO_2Me , R^2 = H +0.89

1g R = H +0.66
1h R = OMe +0.29
1i R = CO_2Me +1.00
1j R = Bpin +0.72

Figure 4. DFT computed one-electron oxidation potentials of N-aryl-pyrrolidines and piperidines (E_{ox} given in V vs. SCE).

The reactions were carried out first at low scale (1 µmol) in TFT with CdS or CdSe QDs using optimized reaction conditions described in Table 3 (entries 1 and 2) and 24–32 hours irradiation times. The results

are collected in Scheme 2. The reaction worked well with the electron-rich *para*-methoxyphenylpyrrolidine **1b**, which has a lower oxidation potential than the parent aniline **1a** (see Figure 4), leading to **4b** in 55% yield using CdS QDs and 65% using CdSe QDs. Similarly, the reactions using the *para*-methylphenylpyrrolidine **1c** and the 2-methyl substituted *N*-phenylpyrrolidine **1d** worked well leading to the final products **4c** and **4d** in 38–62% yields**.** These results are equivalent to those obtained under Ir-photocatalysis.[39] In contrast, *p*-carbomethoxyphenylpyrrolidine **1f** which provides the annulated product in 42% yield under Ir-photocatalysis,[39] did not afford any traces of the desired product with CdS and CdSe QDs dispersed in TFT and **1f** was fully recovered after the irradiation period. The DFT calculations for the oxidation potential of **1f** in TFT (+0.89 V vs. SCE) is presumably out of reach of photogenerated holes in CdS and CdSe QDs explored in this study.

Next, *N*-arylpiperidines were tested and reacted similarly to the corresponding *N*-arylpyrrolidines. Phenylpiperidine (**1g**) provided **4g** in 72% yield under CdS and 70% under CdSe QDs photocatalysis. A similar yield of 67% was previously reported under Ir-photocatalysis.[39] The electron-rich *p*-methoxyphenylpiperidine (**1h**) was converted to **4h** in 48% yield with CdS QDs and 64% with CdSe QDs. As for the pyrrolidine counterpart, the *p*-carbomethoxyphenylpiperidine reacted neither under CdS QDs nor under CdSe QDs photocatalysis. The *N*-(*p*-pinacolborylphenyl)piperidine (**1j**), a substrate that worked well under Ir-photocatalysis,[39] was examined next. It did not provide the annulated product **4j** even though the calculated redox potential (+0.72 V vs. SCE, Figure 4) could have been accessible for the oxidation using CdS QDs. In that case, side reactions leading to homocouplings products could not be excluded as this kind of reactivity was reported und QDs catalysis.[52] However, **1j** was recovered at 40% after 24h of irradiation, so it seems like the redox potential of **1j** is too high for the oxidation using photoexcited CdS and CdSe QDs.

Overall [3+3] annulation reactions with substrates having oxidation potentials up to +0.66 V vs. SCE (**1a**, **1b**, **1c**, **1d**, **1g**, **1h)** were successful with both CdS and CdS QDs, whereas substrates with oxidation potentials higher than +0.72 V. vs. SCE (**1f**, **1i**, **1j**) did not react with photoexcited CdS or CdSe QDs.

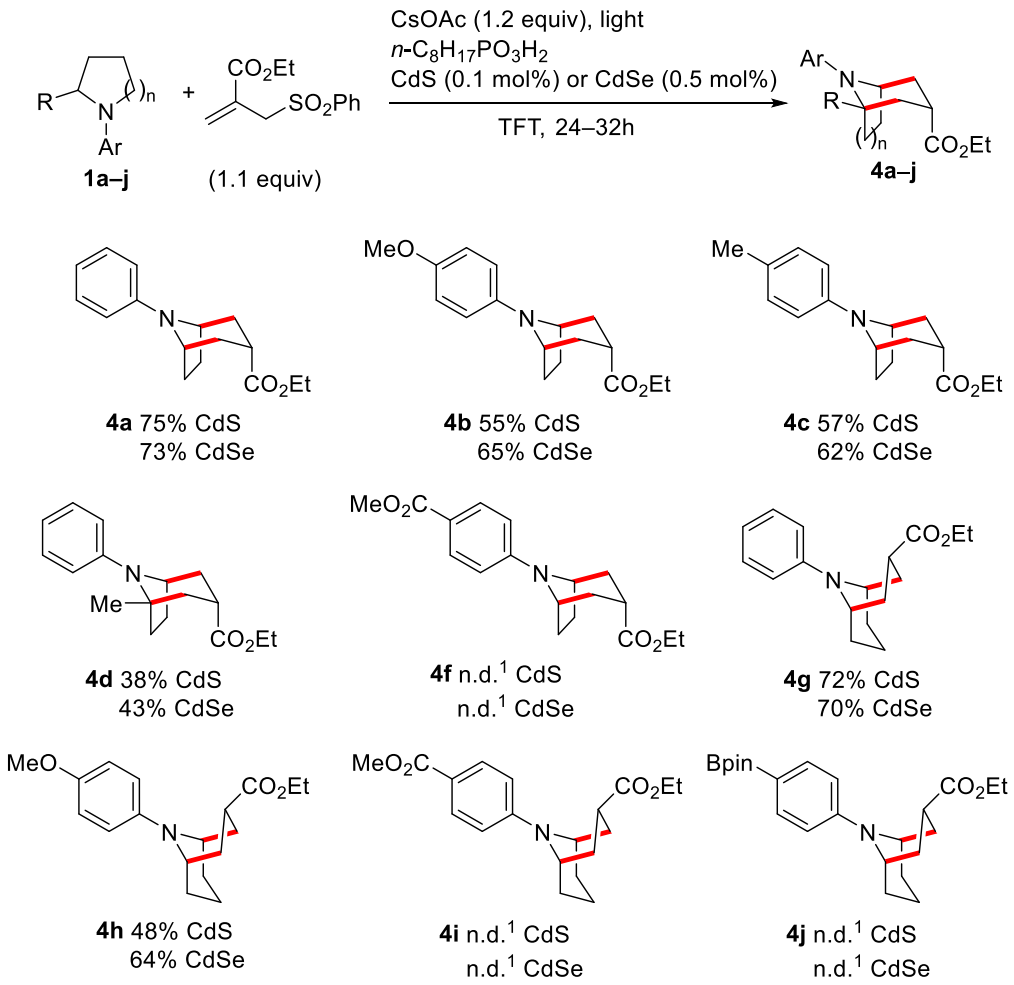

Scheme 2. Reaction scope with *N*-arylamines (1 µmol scale, yields determined by UHPLC-MS).
[1] n.d. = not detected.

Reactions were then repeated on 50 µmol scale with *N*-arylpyrrolidines **1a**–**1e** and the allyl acetate trap (Scheme 3). Products **4a**, **4c** and **4e** were obtained in yields similar to the one obtained under Ir-photocatalysis. Lower yields were observed for the formation of **4b** and **4e**.

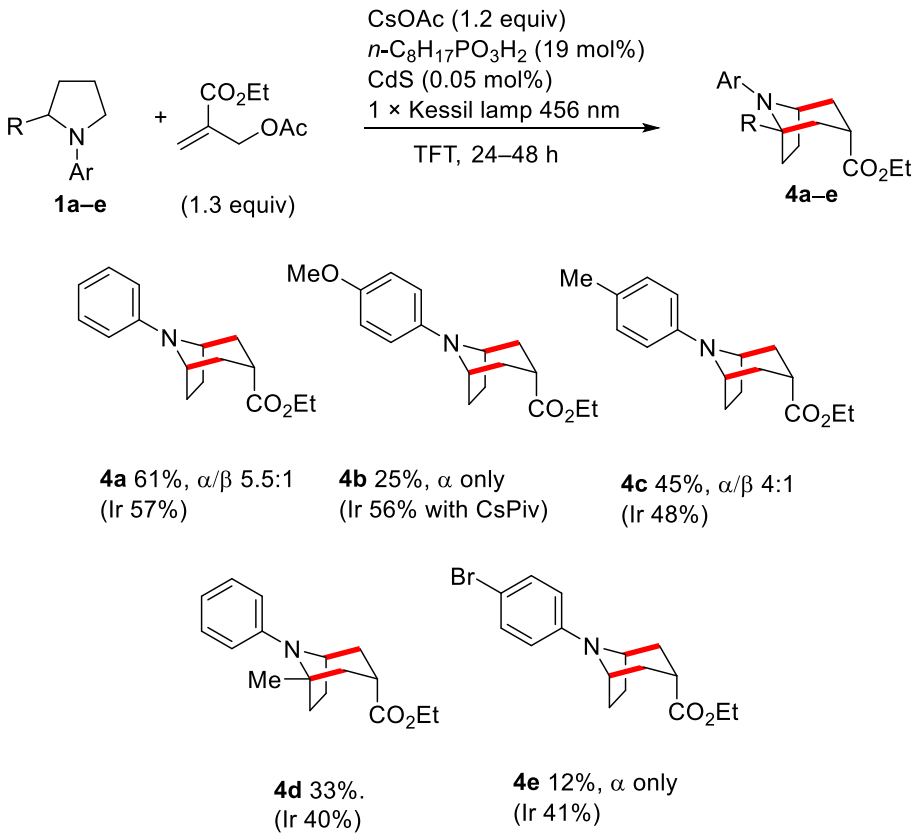

Scheme 3. Substrate scope with *N*-arylpyrrolidines (50 µmol) using CdS QDs. Yields given for the iridium-catalyzed reactions are taken from previous work[39]

Scaling-up reactions with *N*-arylpiperidines was more challenging than expected. *N*-Phenylpiperidine **1g** provided the allylated intermediate **3g** (14%) and the tricyclic compound **5g** (13%) but none the desired bicycle **4g** (Scheme 4). The formation of **5g** suggests that the reduction of the first α-ester radical adduct is slow (see mechanism discussed in Scheme 6). Using the sulfone trap allowed to circumvent this problem since fast β-fragmentation of the benzenesulfonyl radical takes place giving the intermediate allylated product **3g** without the need for a reduction of the α-ester radical adduct (see mechanistic discussion, Scheme 5). Under these conditions, the desired cyclized product **4g** was obtained in 25% yield.

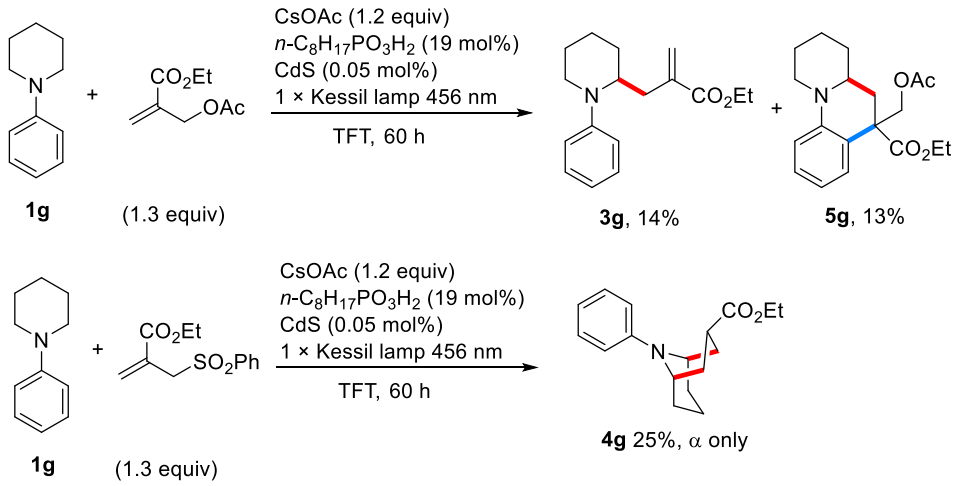

Scheme 4. Reactivity of *N*-phenylpiperidine (**1g**) with CdS quantum dots.

D. Mechanism

Allyl sulfone radical trap

Scheme 5 shows the reaction mechanism proposed for the catalytic cycles involving *N*-phenylpyrrolidne **1a** and the allyl sulfone trap leading to the bicycle **4a**. Under visible light irradiation, the hole in the valence band of the excited **QD[+-]** is able to oxidize **1a** (E_{ox} = 0.64 V vs. SCE in TFT) to its α-amino radical cation **RC1**, which provides the α-amino radical **R1** after deprotonation. Addition of **R1** to the allyl sulfone gives the intermediate α-ester radical **R2** that undergoes fast β-fragmentation of the benzenesulfonyl radical providing the intermediate allylated pyrrolidine **3a**. The first photocatalytic cycle is achieved by reduction of the sulfonyl radical (E_{red} = +0.46 V vs. SCE) to the sulfinate anion by the reduced form of the quantum dot **QD[-]**. The second catalytic cycle involves oxidation of **3a** by the excited quantum dot **QD[+-]** affording the radical cation **RC3** followed by deprotonation to provide the α-aminoalkyl radical **R3**. Then **R3** undergoes a 6-*endo*-trig cyclization, leading to the bicyclic α-ester radical **R4** (calculated E_{red} = –0.77 V vs. SCE). Finally, reduction of the radical **R4** by the reduced form of the quantum dot **QD[-]** closes the second catalytic cycle affording after protonation of the ester enolate the bicyclic product **4a**. Interestingly, despite the fact that **4a** can easily be oxidized by the excited QD[+-] to the **RC4**, this oxidation does not lead to a bicyclic α-aminoalkyl radical due the much lower acidity of the bicyclic radical cation **RC4** (pKa =58.8) relative to the monocyclic one (**RC3** and **RC1**, pKa=51.4 and 52.7, respectively). **RC4** is presumably rapidly converted to **RC3** and **RC1** via electron transfer process with the corresponding amine **3a** and **1a**.[39]

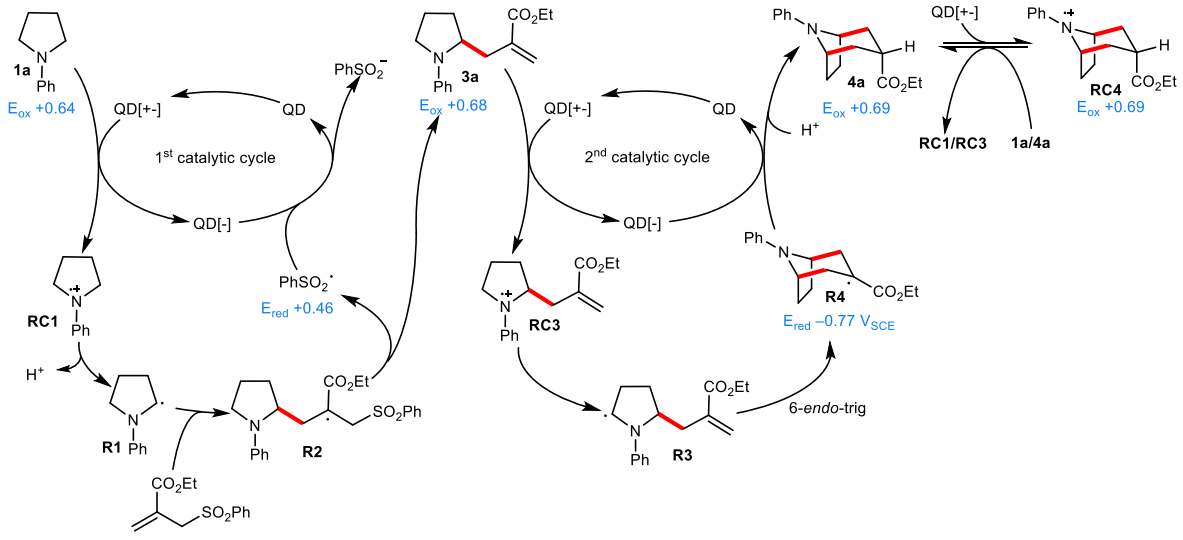

Scheme 5. Mechanism of the allyl sulfone mediated [3+3]-annulation. Calculated redox potentials in V vs. SCE indicated in blue.

Allyl acetate radical trap

When the allylic acetate radical trap is used, the same mechanism is operating, except for the fact that the radical intermediate **R2'** cannot undergo a radical fragmentation but is rather reduced by **QD[-]** to its enolate (E_{red} > –0.29 V vs SCE according to DFT computations), triggering the elimination of an acetate anion. This SET process completes the first catalytic cycle (Scheme 6). Results obtained with the piperidine **1g** (Scheme 4) suggest that the lifetime of radical **R2'** is longer that the one of **R2** (Scheme 5) and therefore side reactions such as intramolecular addition to the *N*-aryl moiety leading to the formation of **5g** was observed when the reaction was run with allyl acetate and could be prevented by using the allyl sulfone trap.

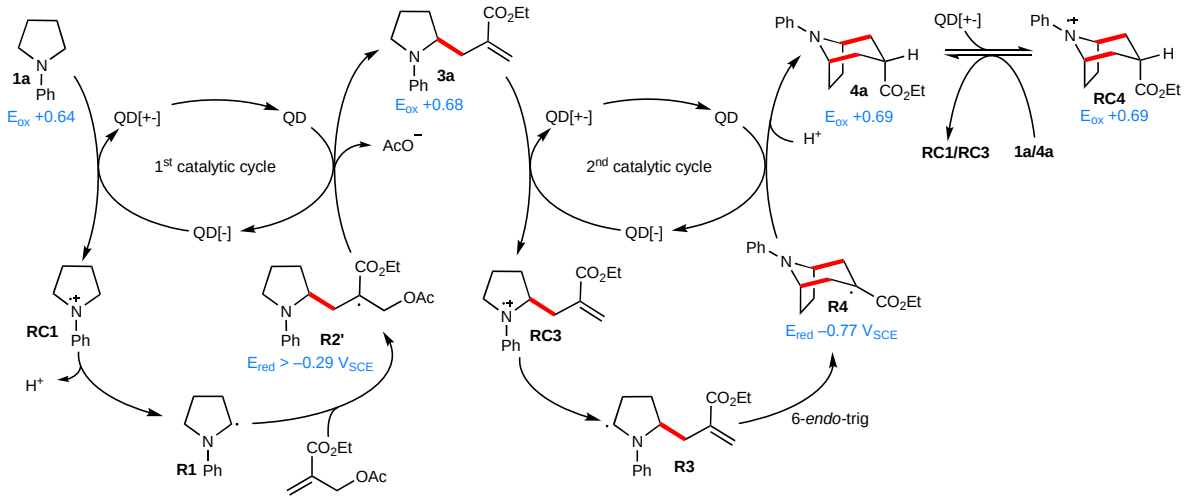

Scheme 6. Mechanism of the allyl acetate mediated [3+3]-annulation. Calculated redox potentials in V vs. SCE indicated in blue.

Effect of the ligands exchange depending on QDs and on the targeted reaction

Overall the partial (or complete) exchange of ligands for three kinds of QDs, namely core CdS, core CdSe and inverted type I core-shell CdS-CdSe enabled to perform both steps of the [3+3] annulation reaction by unlocking the reactivity of QDs for the second cyclization step (see Table 3), which was otherwise very inefficient (see Table 2). Interestingly, the same ligands exchange brought no improvement for the vinylation reaction (see Tables 2 and 3). This suggests that the ligand exchange process specifically helps the cyclization step. The origin of this effect is unclear but the creation of disorder in the ligand layer might provide a better catalyst access to the bulkier and less hydrophobic allylated intermediate product **3a** compared to the initial phenylpyrrolidine **1a**.

Moreover, in these three types of QDs, photogenerated holes are located in the core or the outer shell, which, in both cases is directly in contact with ligands. Other tested core-shell QDs with holes confined in the inner core (CdSe-CdS and InP-ZnS) exhibited no improved reactivity when adding shorter ligands.

Part of the improvement may be due to modification of interaction of the holes with the shorter phosphonate ligands compared with initial oleate and amine ligands.

Photocatalytic activity of the different types QDs: Insights at the mechanistic redox steps

Our results show a clear variation in both efficiency and product selectivity depending on the QDs used. Core CdS and CdSe as well as inverted Type-I CdS-CdSe QDs demonstrate the best photocatalytic activity for the production of the bicyclic amines. This can be rationalized by the better accessibility of the charge carriers (mainly holes in our reactions) which are closer to the surface for these two types of QDs (see Figure 1A and C). These QDs were also able to accomplish the different redox processes required at different stages of the catalytic mechanism due to their suitable oxidation and reduction capabilities. Indeed, theses QDs in their various redox forms are expected to be able to oxidize amines **1a** (E_{ox} = +0.64 V vs. SCE) and **3a** (E_{ox} = +0.68 V vs SCE) and to reduce radical **R2'** (E_{red} > –0.29 V vs. SCE) with the acetate trap, or the benzenesufonyl radical (E_{red} = +0.46 V vs. SCE) with the sulfone trap. Interestingly, reduction of the radical **R4** (E_{red} = –0.77 V vs. SCE) requires a stronger reducing species than the β-acetoxylated α-ester radical **R2'** (E_{red} > –0.29 V vs. SCE). **QD[-]** states of CdS, CdSe and core-shell CdS-CdSe QDs are expected to be reducing enough to reduce **R4** and to close the second catalytic cycle allowing an efficient synthesis of the bicyclic amine **4a**. By taking into account a band gap of 2.7 eV for CdS QDs (460 nm), the position of the conduction band and valence band edges of CdS QDs can be estimated to be in the range E_{CB} = –1.5 to –1.04 V vs. SCE and E_{VB} = +1.2 to +1.66 V vs. SCE. Similarly, CdSe QDs having a band gap of 2.3 eV (540 nm) are expected to have a conduction positioned at E_{CB} = –0.64 to –1.1 V vs. SCE and a valence band at E_{VB} = +0.66 to +1.2 V vs. SCE (see Table 1).

For InP-ZnS QDs, the reaction afforded **3a** without producing the final bicyclic amine **4a**. This indicates that these catalysts are effective for the first catalytic cycle but not for the second one. The conduction band position of the InP-ZnS QDs was previously estimated to be E_{CB} = –0.9 V vs. SCE using electrochemical measurements.[38,42] This value indicates that the reduction of the α-ester radical **R2'** or the benzenesulfonyl (first catalytic cycle) should be easily possible but that the reduction of **R4** (second catalytic cycle, E_{red} = –0.77 V vs. SCE) is challenging for InP-ZnS QDs. Consequently, the first catalytic cycle leading to **3a** is effective but the second catalytic cycle leading to **4a** cannot be achieved. The fact that **3a** could be produced in fair yield indicated that another reduction process is probably involved to regenerate the catalyst when the oxidation of the **3a** takes place (beginning of the second cycle). Presumably, the reduced catalyst **QD[-]** is able to reduce the acrylate radical trap. This non-productive process provides the starting QD in its ground state ready to catalyze the first catalytic cycle.

Conclusion

Core CdS, core CdSe and inverted type I core-shell CdS-CdSe QDs were found to successfully photocatalyze the [3+3]-annulation process involving two successive catalytic cycles leading to tropane derivatives. This is consistent with the good accessibility of the holes in such QDs, which is necessary for the efficient oxidation of the *N*-arylamine substrates. However, the expected localization of both charges in the outer CdSe shell in inverted type I CdS-CdSe does not increase their reactivity compared to core CdS or CdSe QDs. Highest TON were obtained with core CdS QDs. Using this catalyst, the [3+3]-annulation reaction was performed on a scale up to 200 µmol allowing isolation of bicyclic amines closely related to tropanes alkaloids. This work also demonstrates that the photocatalytic activity of QDs for such a complex reaction sequence can be tuned by modification of the QD ligands layer. Partial exchange of the QDs long chain native ligands (oleates and oleylamines) with shorter n-octylphosphonate ligands appeared to be strongly beneficial for performing the second step of the [3+3]-annulation reaction and was achieved by simple addition of n-octylphosphonic acid in the reaction mixture. Interestingly, the use of type I InP-ZnS core-shell QDs enabled to cleanly allylate the *N*-arylpyrrolidine in fair yield without producing the bicyclic compound. This transformation is hardly achievable using Ir-complex photocatalysts.

Overall this study exemplifies the versatility of QDs as redox photocatalysts by showing that they are able to photocatalyze a complex photoredox one-pot two-steps reaction with yields very comparable to Ir-complex photocatalysts. By playing with the composition of the QDs and their ligands layer, it is possible to modulate their reactivity to perform either one or both steps of the process. Remarkably, QDs require very low catalyst loading and preliminary results indicates that recycling of the catalyst may be envisaged.

Experimental part

Quantum Dots Synthesis

CdS[43], CdSe[44], CdSe-CdS[46], CdS-CdSe[25,26], InP[45] and oleylamine coated InP-ZnS[45] QDs were synthesized using hot injection methods following literature procedures with few modifications for each type of Quantum Dots. The detailed synthesis procedures and analyses by TEM, UV-vis absorption spectroscopy, and photoluminescence spectroscopy are described in the SI section S-1. Oleate-capped InP-ZnS core-shell QDs were purchased from NN-Labs (Fayetteville, AR, USA).

Photocatalysis

All the one micromole scale photocatalytic reactions were carried out in a 2ml clear glass screw cap HPLC vial under an inert atmosphere in a nitrogen-filled glovebox. All the stock solutions of the reactions' reagents and the QDs were dissolved in degassed solvents placed in the glovebox. The reaction medium was maintained under continuous stirring using a magnetic stirring bar over the complete irradiation time. The reactions were set for irradiation using the home-made irradiation setup connected to Oslon4 power Star LED source of suitable wavelength (See SI section S7). During the irradiation, 30 µL volume aliquots were taken for the analyses at specific intervals of time during the reaction and analyzed by the UHPLC-MS (see SI section S.9).

For the scale up at the 0.05 mmol and 0.2 mmol scales, the reactions were entirely set up in the glovebox in the appropriate reaction vessels (see SI section S.10). Typically, in the reaction vessel equipped with a stirring bar were added the CdS QDs (20 µM in TFT, 1.250 mL, 0.05 mol%) and the OPAc ligands (50 mM in TFT, 0.190 mL, 19 mol%). Additional TFT was added so that the total end volume of the reaction mixture reached 4 mL (12.5 mM, 2.250 mL). The solution was stirred in the dark in the glovebox for 1 h 30. Then, the starting material (1 M in TFT, 50 µL, 0.05 mmol), the radical trap ethyl 2-(acetoxymethyl)prop-2-enoate (0.250 M in α,α,α-TFT, 0.260 mL, 1.3 equiv.) and CsOAc (12 mg, 1.2 equiv.) were added. The vial was tightly closed. A layer of Teflon tape and parafilm was added around the cap. The vial was taken out of the glovebox for irradiation under a 456 nm Kessil lamp (PR160L) for 24 hours (and 525 nm for experiments using CdSe QDs). A ventilator was used. When a Schlenk tube was used, no Teflon tape and/or parafilm was used. The protocol was unchanged when scaling up the reaction to 0.20 mmol, except that two 456 nm Kessil lamps were used opposite to each other, and the reaction time was doubled. The detailed procedure of work-up, purification and analyses of the reaction product can be found in SI section S.10.

DFT computation

All DFT calculations were performed with the ADF (Amsterdam Density Functional) code developed by E. J. Baerends and co-workers[53] using triple-zeta basis sets (no frozen core). Geometry optimizations were performed *in vacuo* relying on the Generalized Gradient Approximation (GGA) VBP exchange-correlation (XC) potential (VWN + BP: Vosko, Wilk & Nusair[54] + corrective terms by Becke[55] for the exchange, and Perdew[56] for the correlation) with ADF grid precision 6 throughout. The interaction of the molecules with their polarizable (solvent) environment is computed with the COSMO (COnductor-like Screening Model)[57–59] ADF module, representing the solvent as a dielectric continuum. The key parameters for acetonitrile are ε = 37.5 (dielectric constant) and R = 2.76 Å (radius of the rigid sphere solvent molecule). For TFT (trifluorotoluene): ε = 9.2 and R = 3.48 Å. Absolute redox potentials are then

referred to the normal hydrogen electrode (NHE) applying a shift of -4.43 eV defined at pH=0[60]. The shift between NHE and Calomel (SCE) is set at 0.24 V (i.e. $E°_{SCE} = E°_{NHE}$ -0.24 V).

Acknowledgements

This work was supported by the Swiss National Science Foundation (project 200021L_182078) and the ANR (project ANR-18-CE93-0004) under the Lead Agency and International Co-Investigator Scheme. V.M. and J.-M. M. thank the Labex ARCANE (ANR-11-LABX-0003) and CBH-EUR-GS (ANR-17-EURE-0003) for partial funding.

References

(1) Prier, C. K.; Rankic, D. A.; MacMillan, D. W. C. Visible Light Photoredox Catalysis with Transition Metal Complexes: Applications in Organic Synthesis. *Chem. Rev.* **2013**, *113* (7), 5322–5363. https://doi.org/10.1021/cr300503r.

(2) Yoon, T. P.; Ischay, M. A.; Du, J. Visible Light Photocatalysis as a Greener Approach to Photochemical Synthesis. *Nature Chem* **2010**, *2* (7), 527–532. https://doi.org/10.1038/nchem.687.

(3) Shaw, M. H.; Twilton, J.; MacMillan, D. W. C. Photoredox Catalysis in Organic Chemistry. *J. Org. Chem.* **2016**, *81* (16), 6898–6926. https://doi.org/10.1021/acs.joc.6b01449.

(4) Bell, J. D.; Murphy, J. A. Recent Advances in Visible Light-Activated Radical Coupling Reactions Triggered by (i) Ruthenium, (Ii) Iridium and (Iii) Organic Photoredox Agents. *Chem. Soc. Rev.* **2021**, *50* (17), 9540–9685. https://doi.org/10.1039/D1CS00311A.

(5) Tucker, J. W.; Stephenson, C. R. J. Shining Light on Photoredox Catalysis: Theory and Synthetic Applications. *J. O;rg. Chem.* **2012**, *77* (4), 1617–1622. https://doi.org/10.1021/jo202538x.

(6) Koike, T.; Akita, M. Visible-Light Radical Reaction Designed by Ru- and Ir-Based Photoredox Catalysis. *Inorganic Chemistry Frontiers* **2014**, *1* (8), 562–576. https://doi.org/10.1039/C4QI00053F.

(7) Xie, J.; Jin, H.; K. Hashmi, A. S. The Recent Achievements of Redox-Neutral Radical C–C Cross-Coupling Enabled by Visible-Light. *Chemical Society Reviews* **2017**, *46* (17), 5193–5203. https://doi.org/10.1039/C7CS00339K.

(8) Arcudi, F.; Đorđević, L.; Nagasing, B.; Stupp, S. I.; Weiss, E. A. Quantum Dot-Sensitized Photoreduction of CO2 in Water with Turnover Number > 80,000. *J. Am. Chem. Soc.* **2021**. https://doi.org/10.1021/jacs.1c06961.

(9) Wu, H.-L.; Li, X.-B.; Tung, C.-H.; Wu, L.-Z. Semiconductor Quantum Dots: An Emerging Candidate for CO2 Photoreduction. *Advanced Materials* **2019**, *31* (36), 1900709. https://doi.org/10.1002/adma.201900709.

(10) Kuehnel, M. F.; Orchard, K. L.; Dalle, K. E.; Reisner, E. Selective Photocatalytic CO2 Reduction in Water through Anchoring of a Molecular Ni Catalyst on CdS Nanocrystals. *J. Am. Chem. Soc.* **2017**, *139* (21), 7217–7223. https://doi.org/10.1021/jacs.7b00369.

(11) Li, X.-B.; Tung, C.-H.; Wu, L.-Z. Semiconducting Quantum Dots for Artificial Photosynthesis. *Nat Rev Chem* **2018**, *2* (8), 160–173. https://doi.org/10.1038/s41570-018-0024-8.

(12) Burke, R.; Chakraborty, S.; P. McClelland, K.; Jelušić, J.; M. Matson, E.; L. Bren, K.; D. Krauss, T. Light-Driven Hydrogen Production with CdSe Quantum Dots and a Cobalt Glutathione Catalyst. *Chemical Communications* **2021**, *57* (16), 2053–2056. https://doi.org/10.1039/D0CC07364D.

(13) Han, Z.; Qiu, F.; Eisenberg, R.; Holland, P. L.; Krauss, T. D. Robust Photogeneration of H2 in Water Using Semiconductor Nanocrystals and a Nickel Catalyst. *Science* **2012**, *338* (6112), 1321–1324. https://doi.org/10.1126/science.1227775.

(14) Chauviré, T.; Mouesca, J.-M.; Gasparutto, D.; Ravanat, J.-L.; Lebrun, C.; Gromova, M.; Jouneau, P.-H.; Chauvin, J.; Gambarelli, S.; Maurel, V. Redox Photocatalysis with Water-Soluble Core–Shell CdSe-ZnS Quantum Dots. *J. Phys. Chem. C* **2015**, *119* (31), 17857–17866. https://doi.org/10.1021/acs.jpcc.5b04396.

(15) Kodaimati, M. S.; McClelland, K. P.; He, C.; Lian, S.; Jiang, Y.; Zhang, Z.; Weiss, E. A. Viewpoint: Challenges in Colloidal Photocatalysis and Some Strategies for Addressing Them. *Inorg. Chem.* **2018**, *57* (7), 3659–3670. https://doi.org/10.1021/acs.inorgchem.7b03182.

(16) Huang, C.; Li, X.-B.; Tung, C.-H.; Wu, L.-Z. Photocatalysis with Quantum Dots and Visible Light for Effective Organic Synthesis. *Chemistry – A European Journal* **2018**, *24* (45), 11530–11534. https://doi.org/10.1002/chem.201800391.

(17) Yuan, Y.; Jin, N.; Saghy, P.; Dube, L.; Zhu, H.; Chen, O. Quantum Dot Photocatalysts for Organic Transformations. *J. Phys. Chem. Lett.* **2021**, *12* (30), 7180–7193. https://doi.org/10.1021/acs.jpclett.1c01717.

(18) Wang, D.-Y.; Yin, Y.-Y.; Feng, C.-W.; Rukhsana; Shen, Y.-M. Advances in Homogeneous Photocatalytic Organic Synthesis with Colloidal Quantum Dots. *Catalysts* **2021**, *11* (2), 275. https://doi.org/10.3390/catal11020275.

(19) Jiang, Y.; Wang, C.; Rogers, C. R.; Kodaimati, M. S.; Weiss, E. A. Regio- and Diastereoselective Intermolecular [2+2] Cycloadditions Photocatalysed by Quantum Dots. *Nat. Chem.* **2019**, *11* (11), 1034–1040. https://doi.org/10.1038/s41557-019-0344-4.

(20) Jiang, Y.; López-Arteaga, R.; Weiss, E. A. Quantum Dots Photocatalyze Intermolecular [2 + 2] Cycloadditions of Aromatic Alkenes Adsorbed to Their Surfaces via van Der Waals Interactions. *J. Am. Chem. Soc.* **2022**. https://doi.org/10.1021/jacs.2c00833.

(21) Jiang, Y.; Weiss, E. A. Colloidal Quantum Dots as Photocatalysts for Triplet Excited State Reactions of Organic Molecules. *J. Am. Chem. Soc.* **2020**, *142* (36), 15219–15229. https://doi.org/10.1021/jacs.0c07421.

(22) AbouElhamd, A. R.; Al-Sallal, K. A.; Hassan, A. Review of Core/Shell Quantum Dots Technology Integrated into Building's Glazing. *Energies* **2019**, *12* (6), 1058. https://doi.org/10.3390/en12061058.

(23) Vasudevan, D.; Gaddam, R. R.; Trinchi, A.; Cole, I. Core–Shell Quantum Dots: Properties and Applications. *Journal of Alloys and Compounds* **2015**, *636*, 395–404. https://doi.org/10.1016/j.jallcom.2015.02.102.

(24) Maity, P.; Debnath, T.; Ghosh, H. N. Ultrafast Charge Carrier Delocalization in CdSe/CdS Quasi-Type II and CdS/CdSe Inverted Type I Core–Shell: A Structural Analysis through Carrier-Quenching Study. *J. Phys. Chem. C* **2015**, *119* (46), 26202–26211. https://doi.org/10.1021/acs.jpcc.5b08913.

(25) Pan, Z.; Zhang, H.; Cheng, K.; Hou, Y.; Hua, J.; Zhong, X. Highly Efficient Inverted Type-I CdS/CdSe Core/Shell Structure QD-Sensitized Solar Cells. *ACS Nano* **2012**, *6* (5), 3982–3991. https://doi.org/10.1021/nn300278z.

(26) Wang, P.; Wang, M.; Zhang, J.; Li, C.; Xu, X.; Jin, Y. Shell Thickness Engineering Significantly Boosts the Photocatalytic H2 Evolution Efficiency of CdS/CdSe Core/Shell Quantum Dots. *ACS Appl. Mater. Interfaces* **2017**, *9* (41), 35712–35720. https://doi.org/10.1021/acsami.7b07211.

(27) Pu, C.; Peng, X. To Battle Surface Traps on CdSe/CdS Core/Shell Nanocrystals: Shell Isolation versus Surface Treatment. *J. Am. Chem. Soc.* **2016**, *138* (26), 8134–8142. https://doi.org/10.1021/jacs.6b02909.

(28) Caputo, J. A.; Frenette, L. C.; Zhao, N.; Sowers, K. L.; Krauss, T. D.; Weix, D. J. General and Efficient C–C Bond Forming Photoredox Catalysis with Semiconductor Quantum Dots. *J. Am. Chem. Soc.* **2017**, *139* (12), 4250–4253. https://doi.org/10.1021/jacs.6b13379.

(29) Hu, J.; Pu, T.-J.; Xu, Z.-W.; Xu, W.-Y.; Feng, Y.-S. Cadmium Sulfide Quantum-Dot-Photocatalyzed Cascade Cyclization of Functionalized Difluoromethyl Chlorides with Unactivated Olefins. *Advanced Synthesis & Catalysis* **2019**, *361* (4), 708–713. https://doi.org/10.1002/adsc.201801246.

(30) Pal, A.; Ghosh, I.; Sapra, S.; König, B. Quantum Dots in Visible-Light Photoredox Catalysis: Reductive Dehalogenations and C–H Arylation Reactions Using Aryl Bromides. *Chem. Mater.* **2017**, *29* (12), 5225–5231. https://doi.org/10.1021/acs.chemmater.7b01109.

(31) Perez, K. A.; Rogers, C. R.; Weiss, E. A. Quantum Dot-Catalyzed Photoreductive Removal of Sulfonyl-Based Protecting Groups. *Angewandte Chemie International Edition* **2020**, *59* (33), 14091–14095. https://doi.org/10.1002/anie.202005074.

(32) Xi, Z.-W.; Yang, L.; Wang, D.-Y.; Pu, C.-D.; Shen, Y.-M.; Wu, C.-D.; Peng, X.-G. Visible-Light Photocatalytic Synthesis of Amines from Imines via Transfer Hydrogenation Using Quantum Dots as Catalysts. *J. Org. Chem.* **2018**, *83* (19), 11886–11895. https://doi.org/10.1021/acs.joc.8b01651.

(33) Xi, Z.-W.; Yang, L.; Wang, D.-Y.; Feng, C.-W.; Qin, Y.; Shen, Y.-M.; Pu, C.; Peng, X. Visible Light Induced Reduction and Pinacol Coupling of Aldehydes and Ketones Catalyzed by Core/Shell Quantum Dots. *J. Org. Chem.* **2021**, *86* (3), 2474–2488. https://doi.org/10.1021/acs.joc.0c02627.

(34) Huang, C.; Ci, R.-N.; Qiao, J.; Wang, X.-Z.; Feng, K.; Chen, B.; Tung, C.-H.; Wu, L.-Z. Direct Allylic C(Sp3)−H and Vinylic C(Sp2)−H Thiolation with Hydrogen Evolution by Quantum Dots and Visible Light. *Angewandte Chemie International Edition* **2021**, *60* (21), 11779–11783. https://doi.org/10.1002/anie.202101947.

(35) Qiao, J.; Song, Z.-Q.; Huang, C.; Ci, R.-N.; Liu, Z.; Chen, B.; Tung, C.-H.; Wu, L.-Z. Direct, Site-Selective and Redox-Neutral α-C−H Bond Functionalization of Tetrahydrofurans via Quantum Dots Photocatalysis. *Angewandte Chemie International Edition* **2021**, *60* (52), 27201–27205. https://doi.org/10.1002/anie.202109849.

(36) Huang, C.; Qiao, J.; Ci, R.-N.; Wang, X.-Z.; Wang, Y.; Wang, J.-H.; Chen, B.; Tung, C.-H.; Wu, L.-Z. Quantum Dots Enable Direct Alkylation and Arylation of Allylic C(Sp3)–H Bonds with Hydrogen Evolution by Solar Energy. *Chem* **2021**, *7* (5), 1244–1257. https://doi.org/10.1016/j.chempr.2021.01.019.

(37) Zhang, Z.; Edme, K.; Lian, S.; Weiss, E. A. Enhancing the Rate of Quantum-Dot-Photocatalyzed Carbon–Carbon Coupling by Tuning the Composition of the Dot's Ligand Shell. *J. Am. Chem. Soc.* **2017**, *139* (12), 4246–4249. https://doi.org/10.1021/jacs.6b13220.

(38) Chakraborty, I. N.; Roy, S.; Devatha, G.; Rao, A.; Pillai, P. P. InP/ZnS Quantum Dots as Efficient Visible-Light Photocatalysts for Redox and Carbon–Carbon Coupling Reactions. *Chem. Mater.* **2019**, *31* (7), 2258–2262. https://doi.org/10.1021/acs.chemmater.9b00086.

(39) Colson, E.; Andrez, J.; Dabbous, A.; Dénès, F.; Maurel, V.; Mouesca, J.-M.; Renaud, P. Tropane and Related Alkaloid Skeletons via a Radical [3+3]-Annulation Process. *Commun Chem* **2022**, *5* (1), 1–12. https://doi.org/10.1038/s42004-022-00671-x.

(40) Wang, J.; Xia, T.; Wang, L.; Zheng, X.; Qi, Z.; Gao, C.; Zhu, J.; Li, Z.; Xu, H.; Xiong, Y. Enabling Visible-Light-Driven Selective CO2 Reduction by Doping Quantum Dots: Trapping Electrons and Suppressing H2 Evolution. *Angewandte Chemie International Edition* **2018**, *57* (50), 16447–16451. https://doi.org/10.1002/anie.201810550.

(41) Jasieniak, J.; Califano, M.; Watkins, S. E. Size-Dependent Valence and Conduction Band-Edge Energies of Semiconductor Nanocrystals. *ACS Nano* **2011**, *5* (7), 5888–5902. https://doi.org/10.1021/nn201681s.

(42) Yu, S.; Fan, X.-B.; Wang, X.; Li, J.; Zhang, Q.; Xia, A.; Wei, S.; Wu, L.-Z.; Zhou, Y.; Patzke, G. R. Efficient Photocatalytic Hydrogen Evolution with Ligand Engineered All-Inorganic InP and InP/ZnS Colloidal Quantum Dots. *Nat Commun* **2018**, *9* (1), 4009. https://doi.org/10.1038/s41467-018-06294-y.

(43) Zhang, Z.; Rogers, C. R.; Weiss, E. A. Energy Transfer from CdS QDs to a Photogenerated Pd Complex Enhances the Rate and Selectivity of a Pd-Photocatalyzed Heck Reaction. *J. Am. Chem. Soc.* **2020**, *142* (1), 495–501. https://doi.org/10.1021/jacs.9b11278.

(44) Chambrier, I.; Banerjee, C.; Remiro-Buenamañana, S.; Chao, Y.; Cammidge, A. N.; Bochmann, M. Synthesis of Porphyrin–CdSe Quantum Dot Assemblies: Controlling Ligand Binding by Substituent Effects. *Inorg. Chem.* **2015**, *54* (15), 7368–7380. https://doi.org/10.1021/acs.inorgchem.5b00892.

(45) Tessier, M. D.; Dupont, D.; De Nolf, K.; De Roo, J.; Hens, Z. Economic and Size-Tunable Synthesis of InP/ZnE (E = S, Se) Colloidal Quantum Dots. *Chem. Mater.* **2015**, *27* (13), 4893–4898. https://doi.org/10.1021/acs.chemmater.5b02138.

(46) Niu, Y.; Pu, C.; Lai, R.; Meng, R.; Lin, W.; Qin, H.; Peng, X. One-Pot/Three-Step Synthesis of Zinc-Blende CdSe/CdS Core/Shell Nanocrystals with Thick Shells. *Nano Res.* **2017**, *10* (4), 1149–1162. https://doi.org/10.1007/s12274-016-1287-3.

(47) Noble, A.; MacMillan, D. W. C. Photoredox α-Vinylation of α-Amino Acids and *N* -Aryl Amines. *J. Am. Chem. Soc.* **2014**, *136* (33), 11602–11605. https://doi.org/10.1021/ja506094d.

(48) Kodaimati, M. S.; McClelland, K. P.; He, C.; Lian, S.; Jiang, Y.; Zhang, Z.; Weiss, E. A. Viewpoint: Challenges in Colloidal Photocatalysis and Some Strategies for Addressing Them. *Inorg. Chem.* **2018**, *57* (7), 3659–3670. https://doi.org/10.1021/acs.inorgchem.7b03182.

(49) Wang, W.; Banerjee, S.; Jia, S.; Steigerwald, M. L.; Herman, I. P. Ligand Control of Growth, Morphology, and Capping Structure of Colloidal CdSe Nanorods. *Chem. Mater.* **2007**, *19* (10), 2573–2580. https://doi.org/10.1021/cm0705791.

(50) Weidman, M. C.; Nguyen, Q.; Smilgies, D.-M.; Tisdale, W. A. Impact of Size Dispersity, Ligand Coverage, and Ligand Length on the Structure of PbS Nanocrystal Superlattices. *Chem. Mater.* **2018**, *30* (3), 807–816. https://doi.org/10.1021/acs.chemmater.7b04322.

(51) Calzada, R.; Thompson, C. M.; Westmoreland, D. E.; Edme, K.; Weiss, E. A. Organic-to-Aqueous Phase Transfer of Cadmium Chalcogenide Quantum Dots Using a Sulfur-Free Ligand for Enhanced Photoluminescence and Oxidative Stability. *Chem. Mater.* **2016**, *28* (18), 6716–6723. https://doi.org/10.1021/acs.chemmater.6b03106.

(52) Chandrashekar, H. B.; Maji, A.; Halder, G.; Banerjee, S.; Bhattacharyya, S.; Maiti, D. Photocatalyzed Borylation Using Water-Soluble Quantum Dots. *Chem. Commun.* **2019**, *55* (44), 6201–6204. https://doi.org/10.1039/C9CC01737B.

(53) te Velde, G.; Baerends, E. J. Numerical Integration for Polyatomic Systems. *Journal of Computational Physics* **1992**, *99* (1), 84–98. https://doi.org/10.1016/0021-9991(92)90277-6.

(54) Vosko, S. H.; Wilk, L.; Nusair, M. Accurate Spin-Dependent Electron Liquid Correlation Energies for Local Spin Density Calculations: A Critical Analysis. *Canadian Journal of Physics* **1980**, *58*, 1200–1210.

(55) Becke, A. D. Density-Functional Exchange-Energy Approximation with Correct Asymptotic Behavior. *Physical Review A* **1988**, *38*, 3098–3100.

(56) Perdew, J. P. Density-Functional Approximation for the Correlation Energy of the Inhomogeneous Electron Gas. *Physical Review B: Condensed Matter* **1986**, *33*, 8822–8824.

(57) Klamt, A.; Schüürmann, G. COSMO: A New Approach to Dielectric Screening in Solvents with Explicit Expressions for the Screening Energy and Its Gradient. *Journal of the Chemical Society, Perkin Transactions 2* **1993**, *0* (5), 799–805. https://doi.org/10.1039/P29930000799.

(58) Klamt, A. Conductor-like Screening Model for Real Solvents: A New Approach to the Quantitative Calculation of Solvation Phenomena. *J. Phys. Chem.* **1995**, *99* (7), 2224–2235. https://doi.org/10.1021/j100007a062.

(59) Klamt, A.; Jonas, V. Treatment of the Outlying Charge in Continuum Solvation Models. *Journal of Chemical Physics* **1996**, *105*, 9972–9981. https://doi.org/10.1063/1.472829.

(60) Reiss, H.; Heller, A. The Absolute Potential of the Standard Hydrogen Electrode: A New Estimate. *J. Phys. Chem.* **1985**, *89* (20), 4207–4213. https://doi.org/10.1021/j100266a013.